Partial Peptide Dissociation and Binding Groove Plasticity in two Major Histocompatibility Complex Class I Alleles - Differences between Alleles versus Force Field and Sampling Effects

Sebastian Wingbermühle*[a,b] and Lars V. Schäfer[a]

[a] *Theoretical Chemistry, Ruhr University Bochum, Bochum, Germany.*
[b] *Current affiliation: Department of Applied Physics, Science for Life Laboratory, KTH Royal Institute of Technology, Solna, Sweden.*
* *E-mail: sebastian.wingbermuehle@ruhr-uni-bochum.de*

1 Detailed Methods

In this work, the Potentials of Mean Force (PMF) for the dissociation of the peptide N-terminus in the complexes formed by HLA-B*35:01 with the peptide VPLRAMTY (VY8(P5A)) and HLA-B*44:02 with the peptide EEFGRAFSF (EF9) were calculated using Bias Exchange Umbrella Sampling (BEUS) simulations as implemented in GROMACS, version 5.1.4,[1–7] patched with PLUMED, version 2.3.2.[8] The AMBER99SB-disp force field[9] was employed together with the TIP4PD water model.[10]

1.1 Simulation Setup When Starting from the Crystal Structure (HLA-B*35:01 and HLA-B*44:02)

1.1.1 System Preparation

In the crystal structure of the Major Histocompatibility Complex class I (MHC I) HLA-B*35:01 with VY8 (PDB ID: 1A1N), two point mutations were introduced with the program package *PyMol*: the erroneous proline at position 49 in HLA-B*35:01 and the proline at position 5 in the antigenic peptide were mutated to alanine. Moreover, the protonation states of all histidine residues (Tables S1 and S2) were set manually to guarantee that they are identical with the protonation states used in the second BEUS simulation of HLA-B*35:01 described below. For HLA-B*44:02, the coordinates of the crystal structure with PDB ID 1M6O were used as initial configuration.
Next, the two peptide-MHC I complexes (pMHC I) were placed in a rhombic dodecahedron as simulation box such that the minimum distance between all pMHC I atoms and all box edges amounted to 1.6 nm. Subsequently, the energy of the pMHC I was minimized in vacuum without periodic boundary conditions, using 500 steps of steepest descent integration while all bonds and angles were flexible and the non-bonded interactions were calculated employing the group cut-off scheme with a cut-off of 1.0 nm for both Coulomb and Lennard-Jones interactions. The resulting configuration was solvated in TIP4PD water before NaCl was added at a concentration of 150 mM and the system was neutralized with additional Na^+ ions. The energy of the resulting configuration was again minimized using 500 steps of steepest descent integration and keeping all bonds and angles flexible. However, periodic boundary conditions were employed in all spatial directions, and the non-bonded interactions were treated with the Verlet cut-off scheme using Particle-Mesh-Ewald (PME) summation[11] for Coulomb interactions beyond a distance of 1.0 nm. Lennard-Jones interactions were calculated up to a distance of 1.0 nm, the Lennard-Jones potential was shifted such that it amounted to zero at the cut-off, and an analytical correction for interactions beyond this cut-off was added to the energy.

1.1.2 Equilibration

The system was first equilibrated in the NVT ensemble for 10 ns, using the Verlet leap-frog integrator with a time step of 4 fs because the hydrogen atoms of the pMHC I were represented by virtual sites and all bonds and the angles of water molecules were constrained. pMHC I bonds were constrained using one iteration of *LINCS*[12,13] with expansion order six, and water molecules were constrained employing *SETTLE*.[14] Periodic boundary conditions were used in all spatial directions, and the non-bonded interactions were calculated as described for the last energy minimization in the previous section. The positions of all protein heavy atoms were harmonically restrained using a force constant of 1000 $kJmol^{-1}nm^{-2}$.

The temperature was kept constant at 300 K by velocity rescaling with a stochastic term;[15] two thermostats with a time constant $\tau_T = 0.1$ ps were coupled to the pMHC I and to the surrounding water molecules and ions. Initial velocities were drawn from the Maxwell-Boltzmann distribution at 300 K, and energies and configurations were saved to disc every 10 ps. The equilibration was repeated in the NpT ensemble with the same simulation protocol except that the pressure was maintained at 1.0 bar by an isotropic Berendsen barostat[16] with a time constant $\tau_p = 1.6$ ps, using an analytical correction for the pressure accounting for Lennard-Jones interactions beyond the cut-off. Furthermore, the center of mass of the reference coordinates for the position restraints was scaled with the scaling matrix yielded by the Berendsen barostat.

1.1.3 Non-Equilibrium Pulling

To create starting structures for the BEUS simulations, the final configuration of the NpT equilibration was taken, and within 10 ns, the peptide N-terminus was gradually moved to the target distance to the binding groove of the respective umbrella window by non-equilibrium pulling. For the non-equilibrium pulling, the simulation protocol of the NVT equilibration was employed, but position restraints were turned off. For HLA-B*35:01 in complex with VY8(P5A), the center-of-mass distance between the proline at position 2 at the peptide N-terminus and the tyrosine at position 99 in the MHC I binding groove, r_{P2-Y99}, was used as Reaction Coordinate (RC); for HLA-B*44:02 in complex with EF9, the center-of-mass distance between the glutamate at position 2 at the peptide N-terminus and, again, the tyrosine at position 99 in the MHC I binding groove, r_{E2-Y99}, constituted the RC. Starting from the RC value in the crystal structure (0.773 nm for HLA-B*35:01-VY8(P5A) and 0.661 nm for HLA-B*44:02-EF9), the peptide N-terminus was pulled to the distances and at the rates and with the harmonic force constants given in Tables S3 and S4 for HLA-B*35:01 and HLA-B*44:02, respectively.

1.2 Simulation Setup When Starting from the Final Configurations of a Previous BEUS Simulation (HLA-B*35:01)

From the final configurations of the BEUS simulation performed with AMBER99SB*-ILDNP,[17] the heavy atoms of the pMHC I were extracted. As gmx pdb2gmx suggested different histidine protonation states for the distinct umbrella windows, the most frequent protonation state was determined for all histidines in the pMHC I and enforced in all umbrella windows (Table S1). After ensuring that all pMHC I structures were whole, i.e., GROMACS had not combined parts of two or more periodic images in one simulation box, and located in the center of the simulation box, all configurations were placed in a rhombic dodecahedron such that the minimum distance between all pMHC I atoms and all box edges amounted to 1.0 nm, only to find the largest box and use it for all umbrella windows. Subsequently, all pMHC I configurations were solvated in TIP4PD water, and 150 mM NaCl as well as additional Na^+ ions to neutralize the system were added. Special attention was paid to adding exactly the same amount of water molecules and ions in all umbrella windows.

To remove steric clashes between the pMHC I and the surrounding water molecules and ions, the energies of the configurations of all umbrella windows were minimized with 500 steps of steepest descent integration. All bonds and angles were flexible, but the positions of all pMHC I heavy atoms were harmonically restrained using a force constant of $2000\,\mathrm{kJmol^{-1}nm^{-2}}$. Periodic boundary conditions were employed in all spatial directions, and the non-bonded interactions were treated with the Verlet cut-off scheme using Particle-Mesh-Ewald (PME) summation[11] for Coulomb interactions beyond a distance of 1.0 nm. Lennard-Jones interactions were calculated up to a distance of 1.0 nm, the Lennard-Jones potential was shifted such that it amounted to zero at the cut-off, and an analytical correction for interactions beyond this cut-off was added to the energy.

The resulting 24 configurations were equilibrated in the NpT ensemble, using the same simulation parameters as for the NpT equilibration of the starting configurations derived from the crystal structures; only the time constant of the Berendsen barostat was changed to $\tau_p = 2.0$ ps. After the equilibration, the box dimensions of all umbrella windows were set to the box dimensions of the umbrella window that was closest to the average box volume.

Next, the equilibration was repeated in the NVT ensemble for all umbrella windows, employing the same simulation parameters as for the NVT equilibration of the starting configurations derived from the crystal structures.

After checking the total energy, kinetic energy, potential energy, temperature, and pressure in all umbrella windows, the configurations of all umbrella windows were equilibrated to their respective umbrella restraint for 50 ns. To this end, the simulation parameters used for the NVT equilibration were extended as follows: the center-of-mass distance between the proline at position 2 at the peptide N-terminus and the tyrosine at position 99 in the MHC I binding groove, r_{P2-Y99}, was specified as RC, and the targeted RC values and harmonic force constants given in Table S5 were employed. Last, the

RC value for the final configuration of this equilibration step was calculated in each umbrella window, and configurations were assigned to the umbrella window whose targeted RC value they matched most closely. Therefore, the configurations used as starting structures for umbrella windows $1-24$ in the BEUS simulation were the final configurations of the equilibration umbrella windows 1, 2, 3, 5, 6, 4, 7, 8, 9, 10, 11, 12, 13, 14, 15, 17, 16, 18, 19, 21, 20, 22, 23, and 24.

1.3 BEUS Simulations

Before starting the full-length BEUS simulations, small test runs, 10 ns to 50 ns long, but with the same simulation parameters else, were launched for the sets of starting configurations derived from the crystal structures. At the end of the test run, the transition matrix and the histogram of RC values were checked to verify that exchange probabilities between all replicas ranged between 15 % and 20 % and that the peaks of the histograms of the RC values were located approximately at the targeted value while the histograms of all neighboring umbrella windows overlapped. If one of the criteria was not met, the targeted RC values and the harmonic force constants of the umbrella windows causing the deviation were slightly modified, and a new test run was carried out. This optimization procedure yielded the targeted RC values and harmonic force constants listed in Tables S6 and S7 for HLA-B*35:01 and HLA-B*44:02, respectively. For HLA-B*44:02, the targeted RC values of some umbrella windows were altered sufficiently to justify taking the final configuration of a different umbrella window of the non-equilibrium pulling step as starting structure. Therefore, the 24 umbrella windows of the BEUS simulation correspond to the pulling umbrella windows 1, 2, 3, 4, 6, 8, 9, 9, 10, 10, 11, 11, 11, 12, 12, 13, 14, 15, 16, 17, 18, 19, 20, 21. For the BEUS simulation of HLA-B*35:01 launched from the final configurations of the BEUS simulation performed with AMBER99SB*-ILDNP,[17] the set of targeted RC values and harmonic force constants employed in the previous simulation was used without further optimization (Table S5).

In the BEUS simulations, which were performed in the NVT ensemble, the simulation parameters of the non-equilibrium pulling step were re-used; only the pull rate was set to $0\,\mathrm{nmps}^{-1}$, and the targeted RC values and harmonic force constants were set to the values referenced above. Configurational exchanges between neighboring umbrella windows were attempted every 2 ps and accepted or rejected on the basis of the Metropolis Monte Carlo criterion. Both BEUS simulations of HLA-B*35:01 were carried out for $1\,\mu$s per umbrella window; each umbrella window of the BEUS simulation of HLA-B*44:02 covers 950 ns.

The transition matrices and the histograms of RC values obtained in the three BEUS simulations are listed in Tables S8 − S10 and shown in Figure S1, respectively.

1.4 Analyses

1.4.1 PMF calculation

The PMF at 300 K for the dissociation of the peptide N-terminus, using r_{P2-Y99} and r_{E2-Y99} as RC for HLA-B*35:01 and HLA-B*44:02, respectively, was calculated with gmx wham.[18] Statistical uncertainties were estimated with 200 cycles of bootstrapping during which the PMF was re-computed for new random trajectories with properly distributed and autocorrelated configurations. The first 10 ns in each umbrella window were discarded as additional equilibration time. Series of PMFs calculated for fractions of as well as the full-length trajectories illustrate the convergence of the free-energy profiles (Figure S2).

1.4.2 Distances between Helix Segments

To judge the plasticity of the A-pocket region of the MHC I binding groove both when hosting the respective peptide N-terminus and after its dissociation, eight center-of-mass distances between the C_α-atoms of segments of six residues on opposite binding groove helices were calculated. As the fold of the binding groove is very similar for both alleles studied, the segments selected for both HLA-B*35:01 and HLA-B*44:02 were residues $59-64$ and $65-70$ on the α_1-helix and residues $152-157$, $158-163$, $164-169$, and $170-175$ on the α_2-helix. The corresponding histograms are shown in Figures S4 − S11. Moreover, the average of these distances and its histogram were computed (Figure 3). For all distance calculations, the first 10 ns in each umbrella window were discarded as additional equilibration time.

1.4.3 Configurational Entropy

After a prinicipal component analysis with gmx covar, the configurational entropies of the MHC I binding groove, the antigenic peptide, and the binding groove together with the peptide were computed for all three BEUS simulations using gmx

anaeig (Figures 4, S12 & S13). In the Quasi-Harmonic Approximation (QHA) suggested by Schlitter,[19] the configurational entropy S_{conf} can be shown not to exceed the following upper bound:

$$S_{conf} < 0.5\, k_B \ln\left[\det\left(\mathbf{1} + k_B T e^2 \hbar^{-2} \mathbf{M}^{1/2}\mathbf{C}\mathbf{M}^{1/2}\right)\right], \tag{1}$$

where k_B denotes Boltzmann's constant, T the temperature, e Euler's number, and $\hbar$ the reduced Planck constant. $\mathbf{M}$ is the diagonal matrix of the particle masses, and $\mathbf{C}$ denotes the covariance matrix of the particle positions. Here, $\mathbf{C}$ was computed on the basis of the positions $\tilde{x}$ of all C_α-atoms in the MHC I binding groove and/or the antigenic peptide as:

$$\mathbf{C} = \left\langle (\tilde{x} - \langle \tilde{x} \rangle)\,(\tilde{x} - \langle \tilde{x} \rangle)^T \right\rangle. \tag{2}$$

For the Schlitter entropies, the flexible loops of the binding groove were excluded such that, for both HLA-B*35:01 and HLA-B*44:02, only residues $4-11$, $23-36$, $46-85$, $93-101$, $112-118$, $122-126$ and $137-180$ were considered to be part of the binding groove. Again, the first 10 ns in each umbrella window were discarded as additional equilibration time.

Table S1 Protonation states in the three BEUS simulations of HLA-B*35:01. Because arginine and lysine side chains were always positively charged/protonated and aspartate and glutamate side chains were always negatively charged/deprotonated, only the protonation states of histidine side chains are given below.

Protein	Residue	AMBER99SB*-ILDNP	AMBER99SB-disp (final structures of AMBER99SB*-ILDNP)	AMBER99SB-disp (crystal structure)
HLA	H3	proton at N_δ	proton at N_ε	proton at N_ε
HLA	H93	proton at N_δ	proton at N_ε	proton at N_ε
HLA	H113	proton at N_ε	proton at N_ε	proton at N_ε
HLA	H188	proton at N_ε	proton at N_ε	proton at N_ε
HLA	H191	proton at N_ε	proton at N_ε	proton at N_ε
HLA	H192	proton at N_ε	proton at N_ε	proton at N_ε
HLA	H197	proton at N_ε	proton at N_ε	proton at N_ε
HLA	H260	proton at N_ε	proton at N_ε	proton at N_ε
HLA	H263	proton at N_ε	proton at N_ε	proton at N_ε
β_2m	H13	proton at N_ε	proton at N_ε	proton at N_ε
β_2m	H31	proton at N_ε	proton at N_ε	proton at N_ε
β_2m	H51	proton at N_δ	proton at N_ε	proton at N_ε
β_2m	H84	proton at N_ε	proton at N_δ and N_ε	proton at N_δ and N_ε

Table S2 Protonation states in the BEUS simulation of HLA-B*44:02. Because arginine and lysine side chains were always positively charged/protonated and aspartate and glutamate side chains were always negatively charged/deprotonated, only the protonation states of histidine side chains are given below.

Protein	Residue	AMBER99SB-disp
HLA	H3	proton at N_δ
HLA	H93	proton at N_δ
HLA	H113	proton at N_ε
HLA	H188	proton at N_ε
HLA	H191	proton at N_ε
HLA	H192	proton at N_ε
HLA	H197	proton at N_ε
HLA	H260	proton at N_ε
HLA	H263	proton at N_ε
β_2m	H13	proton at N_ε
β_2m	H31	proton at N_ε
β_2m	H51	proton at N_δ
β_2m	H84	proton at N_δ and N_ε

Table S3 Parameters of the pulling simulation starting from the crystal structure of HLA-B*35:01 and yielding the starting structures for the BEUS simulation.

Window	Targeted r_{P2-Y99} [nm]	Pull rate $[10^{-4}\mathrm{nm} * \mathrm{ps}^{-1}]$	Harmonic force constants $[\mathrm{kJ} * \mathrm{mol}^{-1} * \mathrm{nm}^{-2}]$
1	0.665	-0.108	10000
2	0.790	0.017	10000
3	0.850	0.077	10000
4	0.905	0.132	10000
5	0.960	0.187	10000
6	1.010	0.237	10000
7	1.053	0.280	10000
8	1.100	0.327	10000
9	1.178	0.405	10000
10	1.275	0.502	10000
11	1.372	0.599	10000
12	1.472	0.699	10000
13	1.577	0.804	10000
14	1.677	0.904	10000
15	1.770	0.997	10000
16	1.853	1.080	10000
17	1.942	1.169	10000
18	2.045	1.272	10000
19	2.145	1.372	10000
20	2.244	1.471	10000
21	2.334	1.561	10000
22	2.430	1.657	10000
23	2.530	1.757	10000
24	2.633	1.860	10000

Table S4 Parameters of the pulling simulation starting from the crystal structure of HLA-B*44:02 and yielding the starting structures for the BEUS simulation.

Window	Targeted r_{E2-Y99} [nm]	Pull rate $[10^{-4} nm * ps^{-1}]$	Harmonic force constants $[kJ * mol^{-1} * nm^{-2}]$
1	0.553	-0.108	10000
2	0.678	0.017	10000
3	0.738	0.077	10000
4	0.793	0.132	10000
5	0.848	0.187	10000
6	0.898	0.237	10000
7	0.941	0.280	10000
8	0.988	0.327	10000
9	1.066	0.405	10000
10	1.163	0.502	10000
11	1.260	0.599	10000
12	1.360	0.699	10000
13	1.465	0.804	10000
14	1.565	0.904	10000
15	1.658	0.997	10000
16	1.741	1.080	10000
17	1.830	1.169	10000
18	1.933	1.272	10000
19	2.033	1.372	10000
20	2.132	1.471	10000
21	2.222	1.561	10000
22	2.318	1.657	10000
23	2.418	1.757	10000
24	2.521	1.860	10000

Table S5 Targeted values of the reaction coordinate and harmonic force constants in the BEUS simulation of HLA-B*35:01 started from the final configurations of the BEUS simulation performed with AMBER99SB*-ILDNP.[17]

Window	Targeted r_{P2-Y99} [nm]	Harmonic force constants $[kJ * mol^{-1} * nm^{-2}]$
1	0.665	1000
2	0.790	1000
3	0.900	1000
4	0.942	1300
5	0.970	1500
6	1.010	1500
7	1.053	1200
8	1.100	900
9	1.173	600
10	1.280	500
11	1.372	500
12	1.472	500
13	1.577	500
14	1.677	500
15	1.770	500
16	1.853	500
17	1.942	500
18	2.045	500
19	2.145	500
20	2.244	500
21	2.334	500
22	2.430	500
23	2.530	500
24	2.633	500

Table S6 Targeted values of the reaction coordinate and harmonic force constants in the BEUS simulation of HLA-B*35:01 started from the crystal structure.

Window	Targeted r_{P2-Y99} [nm]	Harmonic force constants $[kJ * mol^{-1} * nm^{-2}]$
1	0.665	1000
2	0.795	1000
3	0.865	1000
4	0.925	1300
5	0.955	1500
6	1.005	1500
7	1.050	1200
8	1.100	900
9	1.178	600
10	1.275	500
11	1.372	500
12	1.472	500
13	1.577	500
14	1.677	500
15	1.767	500
16	1.853	500
17	1.942	500
18	2.045	500
19	2.145	500
20	2.244	500
21	2.334	500
22	2.430	500
23	2.530	500
24	2.633	500

Table S7 Targeted values of the reaction coordinate and harmonic force constants in the BEUS simulation of HLA-B*44:02 started from the crystal structure.

Window	Targeted r_{E2-Y99} [nm]	Harmonic force constants $[kJ * mol^{-1} * nm^{-2}]$
1	0.606	1300
2	0.709	1300
3	0.797	1300
4	0.876	1500
5	0.956	1500
6	0.997	1800
7	1.027	2100
8	1.068	2000
9	1.119	1800
10	1.150	2200
11	1.181	2200
12	1.228	1800
13	1.273	1800
14	1.316	1500
15	1.369	900
16	1.454	600
17	1.559	600
18	1.649	500
19	1.736	500
20	1.827	500
21	1.926	500
22	2.029	500
23	2.126	500
24	2.222	500

Table S8 Exchange probabilities observed in the BEUS simulation of HLA-B*35:01 started from the final configurations of the BEUS simulation performed with AMBER99SB*-ILDNP.[17]

Window	$P_{exchange}$(lower neighbor)	P_{stay}	$P_{exchange}$(upper neighbor)
1	–	0.8067	0.1933
2	0.1933	0.7440	0.0628
3	0.0628	0.6858	0.2514
4	0.2514	0.3913	0.3573
5	0.3573	0.3722	0.2705
6	0.2705	0.5297	0.1998
7	0.1998	0.6077	0.1925
8	0.1925	0.6339	0.1736
9	0.1736	0.6960	0.1305
10	0.1305	0.6956	0.1739
11	0.1739	0.6560	0.1701
12	0.1701	0.6552	0.1747
13	0.1747	0.6256	0.1997
14	0.1997	0.6447	0.1556
15	0.1556	0.6558	0.1887
16	0.1887	0.6311	0.1802
17	0.1802	0.6700	0.1498
18	0.1498	0.6873	0.1629
19	0.1629	0.6755	0.1616
20	0.1616	0.6499	0.1884
21	0.1884	0.6351	0.1765
22	0.1765	0.6483	0.1752
23	0.1752	0.6449	0.1799
24	0.1799	0.8201	–

Table S9 Exchange probabilities observed in the BEUS simulation of HLA-B*35:01 started from the crystal structure.

Window	$P_{exchange}$(lower neighbor)	P_{stay}	$P_{exchange}$(upper neighbor)
1	–	0.8043	0.1957
2	0.1957	0.5348	0.2695
3	0.2695	0.6062	0.1244
4	0.1244	0.6279	0.2477
5	0.2477	0.5447	0.2076
6	0.2076	0.5602	0.2323
7	0.2323	0.6190	0.1487
8	0.1487	0.6926	0.1586
9	0.1586	0.6360	0.2054
10	0.2054	0.6093	0.1853
11	0.1853	0.6493	0.1654
12	0.1654	0.6526	0.1820
13	0.1820	0.6720	0.1460
14	0.1460	0.6845	0.1696
15	0.1696	0.6247	0.2057
16	0.2057	0.5971	0.1972
17	0.1972	0.6640	0.1388
18	0.1388	0.7084	0.1528
19	0.1528	0.6783	0.1689
20	0.1689	0.6464	0.1847
21	0.1847	0.6441	0.1711
22	0.1711	0.6601	0.1687
23	0.1687	0.6566	0.1747
24	0.1747	0.8253	–

Table S10 Exchange probabilities observed in the BEUS simulation of HLA-B*44:02 started from the crystal structure.

Window	$P_{exchange}$(lower neighbor)	P_{stay}	$P_{exchange}$(upper neighbor)
1	–	0.8275	0.1725
2	0.1725	0.6732	0.1543
3	0.1543	0.7670	0.0787
4	0.0787	0.8326	0.0887
5	0.0887	0.7216	0.1897
6	0.1897	0.5296	0.2807
7	0.2807	0.5066	0.2127
8	0.2127	0.6202	0.1671
9	0.1671	0.5679	0.2651
10	0.2651	0.4865	0.2484
11	0.2484	0.5792	0.1724
12	0.1724	0.6386	0.1890
13	0.1890	0.6208	0.1902
14	0.1902	0.6346	0.1752
15	0.1752	0.6555	0.1693
16	0.1693	0.6842	0.1465
17	0.1465	0.6727	0.1809
18	0.1809	0.6423	0.1769
19	0.1769	0.6573	0.1659
20	0.1659	0.6922	0.1420
21	0.1420	0.6813	0.1767
22	0.1767	0.6454	0.1779
23	0.1779	0.6661	0.1560
24	0.1560	0.8440	–

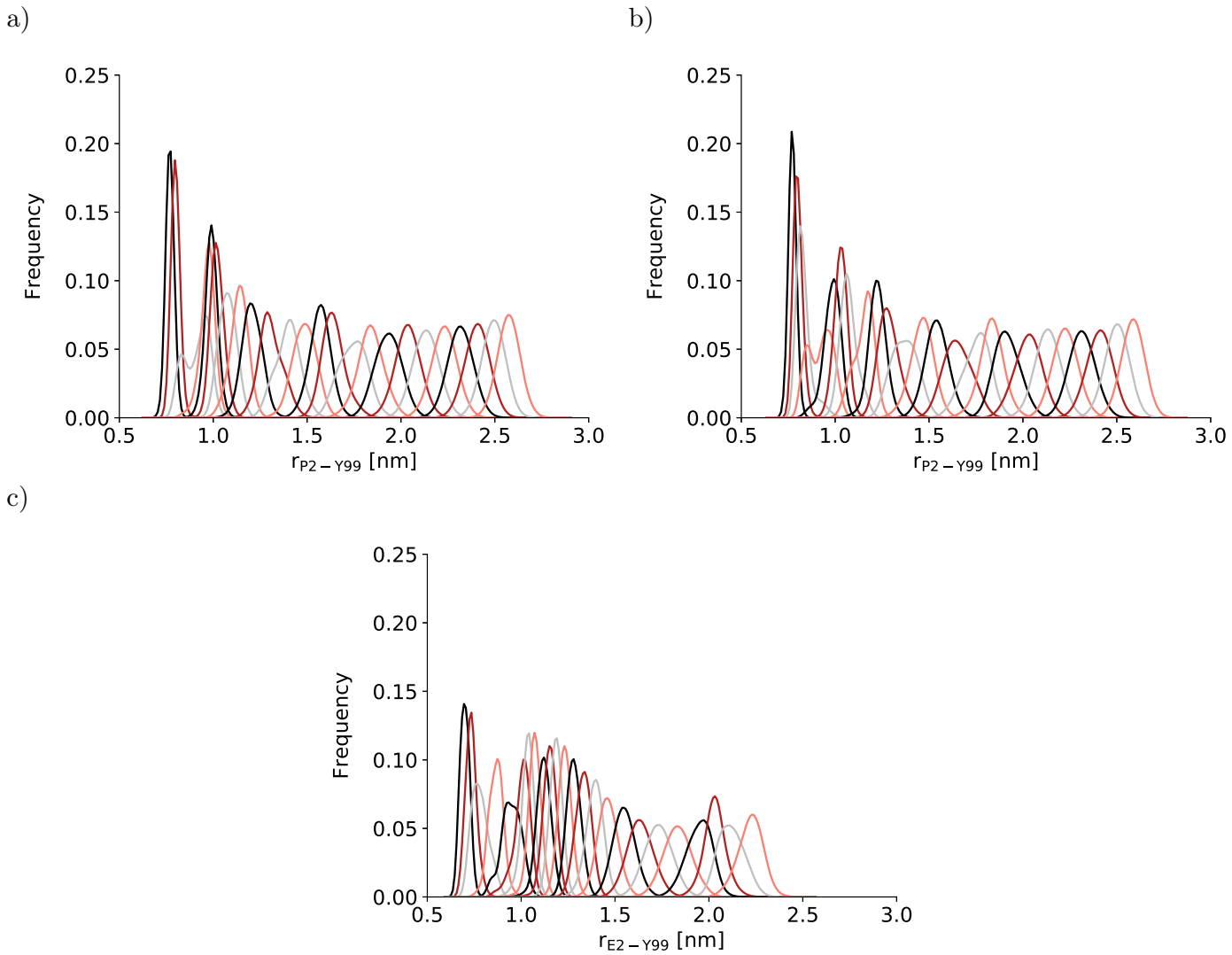

Fig. S1 Histograms of the reaction coordinate value in all umbrella windows of the three BEUS simulations: a) HLA-B*35:01 (starting from the final structures of the BEUS simulation performed with AMBER99SB*-ILDNP[17]), b) HLA-B*35:01 (starting from the crystal structure), and c) HLA-B*44:02 (starting from the crystal structure).

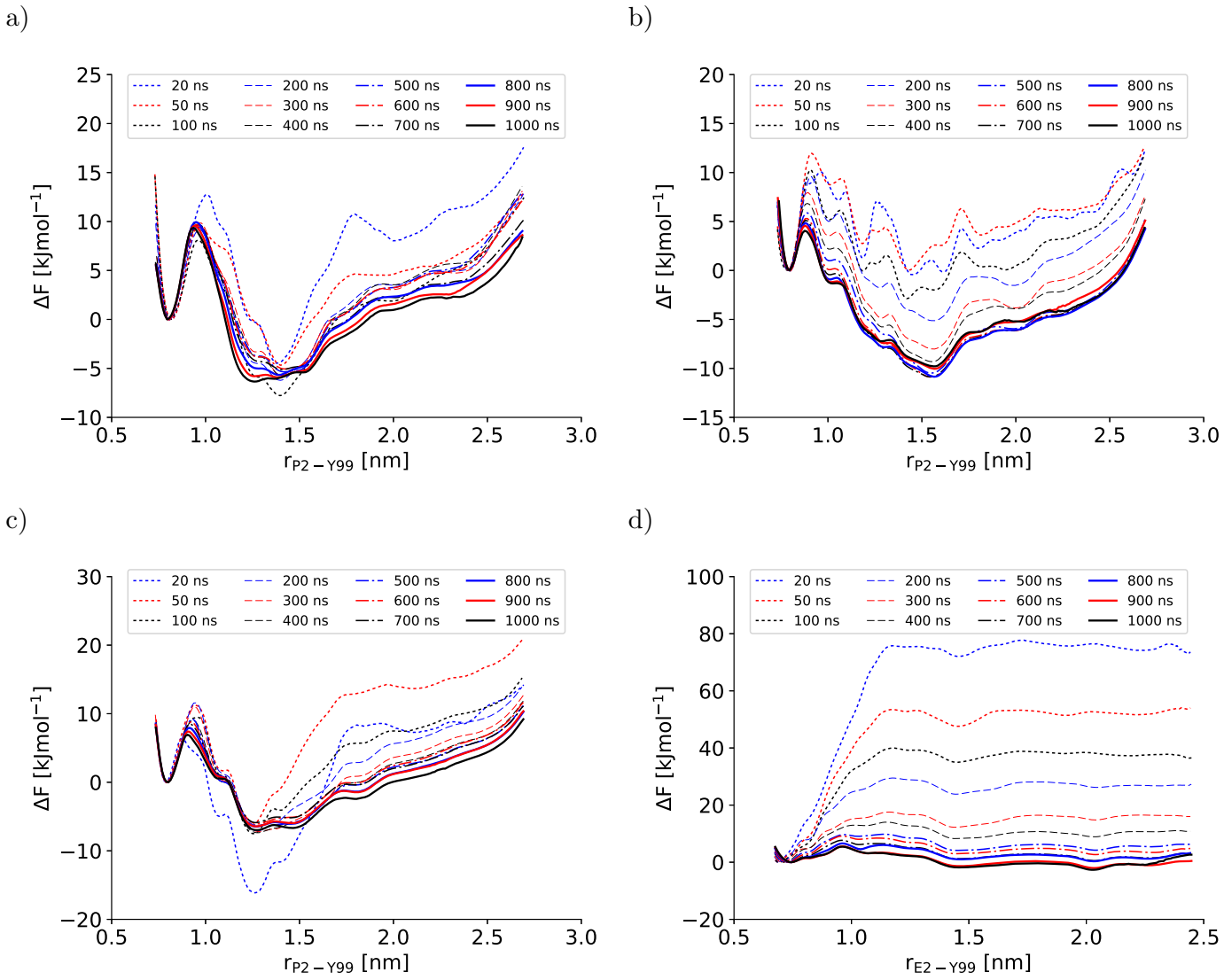

Fig. S2 Convergence of the Potentials of Mean Force (PMFs) for a) HLA-B*35:01 (AMBER99SB*-ILDNP),[17] b) HLA-B*35:01 (AMBER99SB-disp, starting from the final structures of a), c) HLA-B*35:01 (AMBER99SB-disp, starting from the crystal structure), and d) HLA-B*44:02 (AMBER99SB-disp, starting from the crystal structure). In all PMF calculations, the first 10 ns were discarded as equilibration time.

2 Distances Between Binding Groove Helix Segments

In this section, the sextet distances used are plotted on the binding grooves of both HLA-B*35:01 and HLA-B*44:02, illustrating that the binding groove architectures of the two alleles are so similar that, for both alleles, the selected distances are representative of the binding groove's plasticity in the A-pocket region hosting the peptide N-terminus (Figure S3). Next, the distributions of all eight pair distances constituting the average distance presented in Figure 3 are shown in Figures S4 - S11.

a) b)

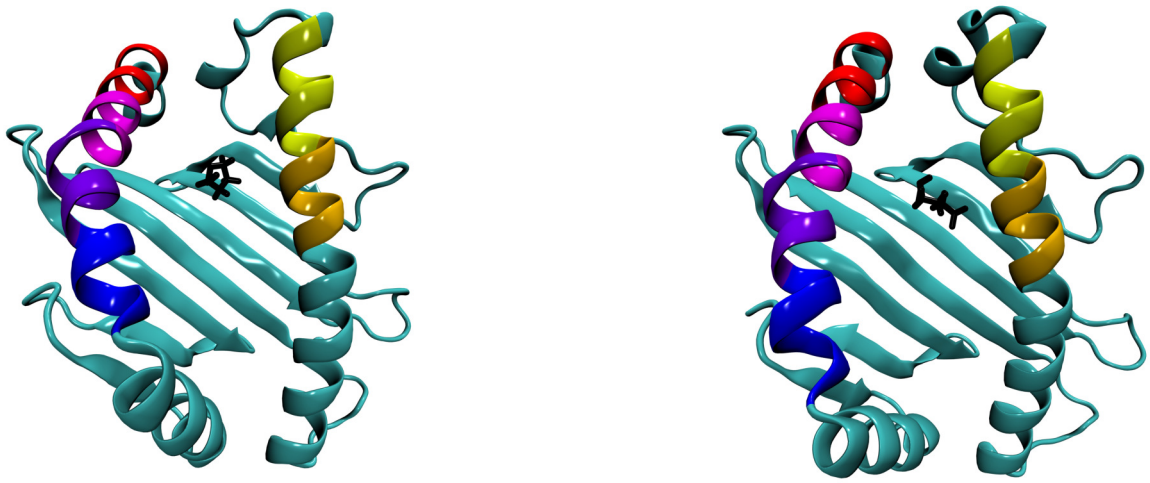

Fig. S3 The binding grooves of a) HLA-B*35:01 and b) HLA-B*44:02. For the sake of clarity, the antigenic peptide has been omitted and the position of the peptide N-terminus is indicated by the anchor reside P2 (black, left) for HLA-B*35:01 or E2 (black, right) for HLA-B*44:02. To judge the biding groove's plasticity, eight pair distances between the centers of mass of the C_α atoms of sextets of residues on opposite binding groove helices were calculated. These sextet distances were computed for residues $59-64$ (yellow) and $65-70$ (orange) on the α_1-helix and residues $152-157$ (blue), $158-163$ (violet), $164-169$ (magenta), and $170-175$ (red) on the α_2-helix.

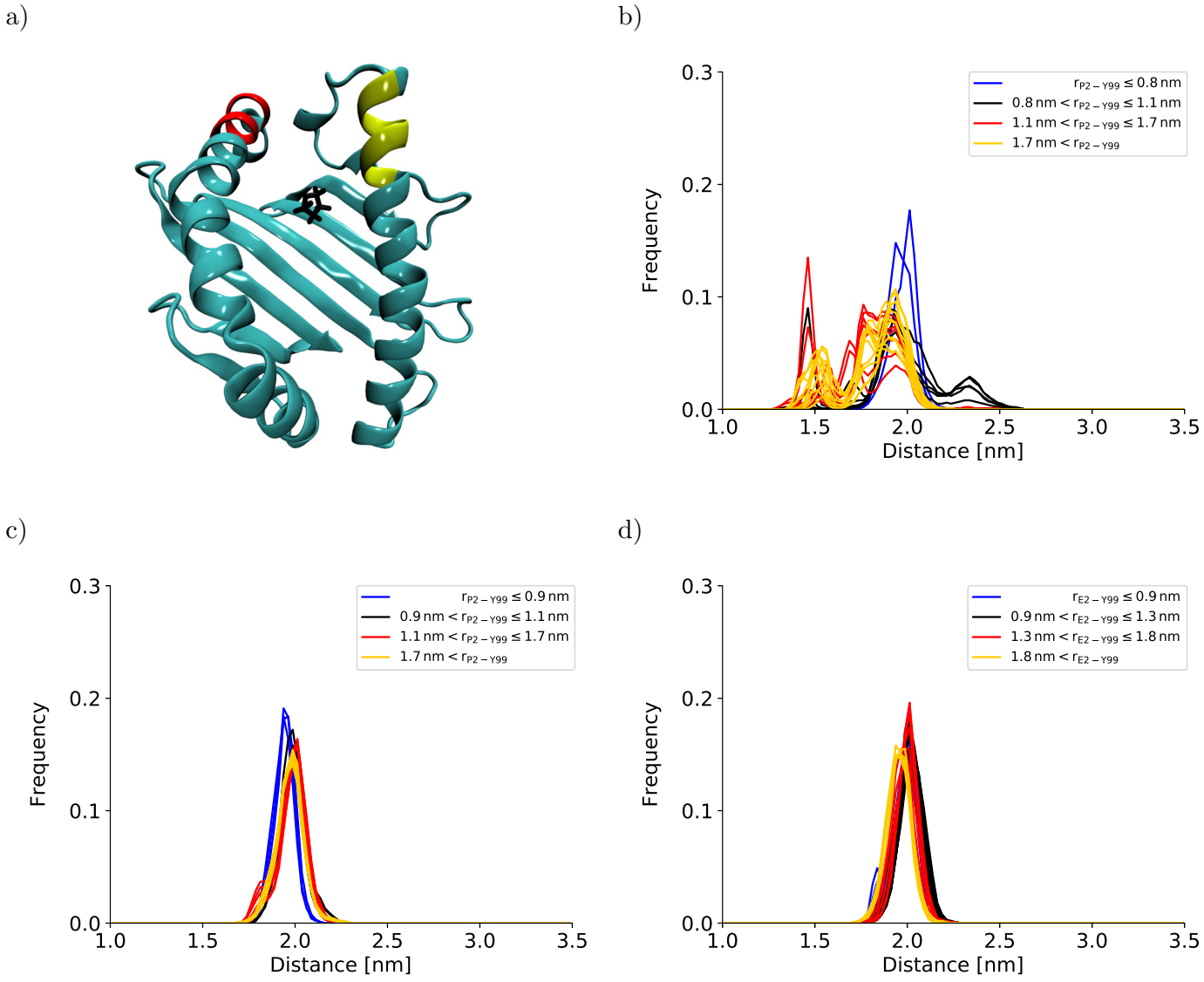

Fig. S4 Sextet distance between residues $59-64$ on the α_1-helix and residues $170-175$ on the α_2-helix. The position of the sextets in the binding groove of HLA-B*35:01 is depicted in a). The histograms of distances are shown for b) HLA-B*35:01 (starting from the final structures of the BEUS simulation performed with AMBER99SB*-ILDNP[17]), c) HLA-B*35:01 (starting from the crystal structure), and d) HLA-B*44:02 (starting from the crystal structure). Histograms shown in blue represent umbrella windows of the fully bound state, histograms in black belong to the barrier region of the PMF, and histograms in red and yellow belong to the adjacent and distant half of the partially dissociated state, respectively.

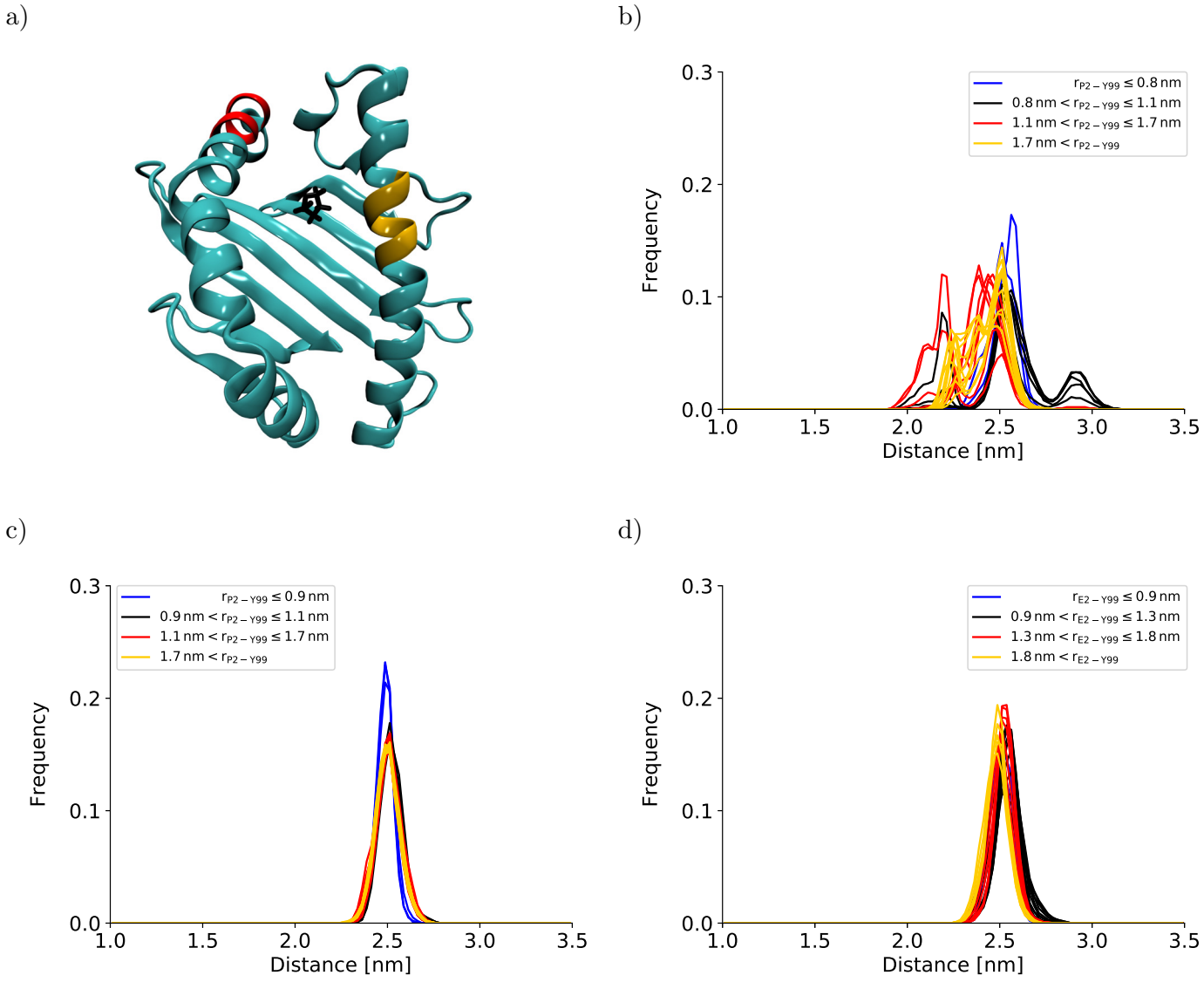

Fig. S5 Sextet distance between residues $65-70$ on the α_1-helix and residues $170-175$ on the α_2-helix. The position of the sextets in the binding groove of HLA-B*35:01 is depicted in a). The histograms of distances are shown for b) HLA-B*35:01 (starting from the final structures of the BEUS simulation performed with AMBER99SB*-ILDNP[17]), c) HLA-B*35:01 (starting from the crystal structure), and d) HLA-B*44:02 (starting from the crystal structure). Histograms shown in blue represent umbrella windows of the fully bound state, histograms in black belong to the barrier region of the PMF, and histograms in red and yellow belong to the adjacent and distant half of the partially dissociated state, respectively.

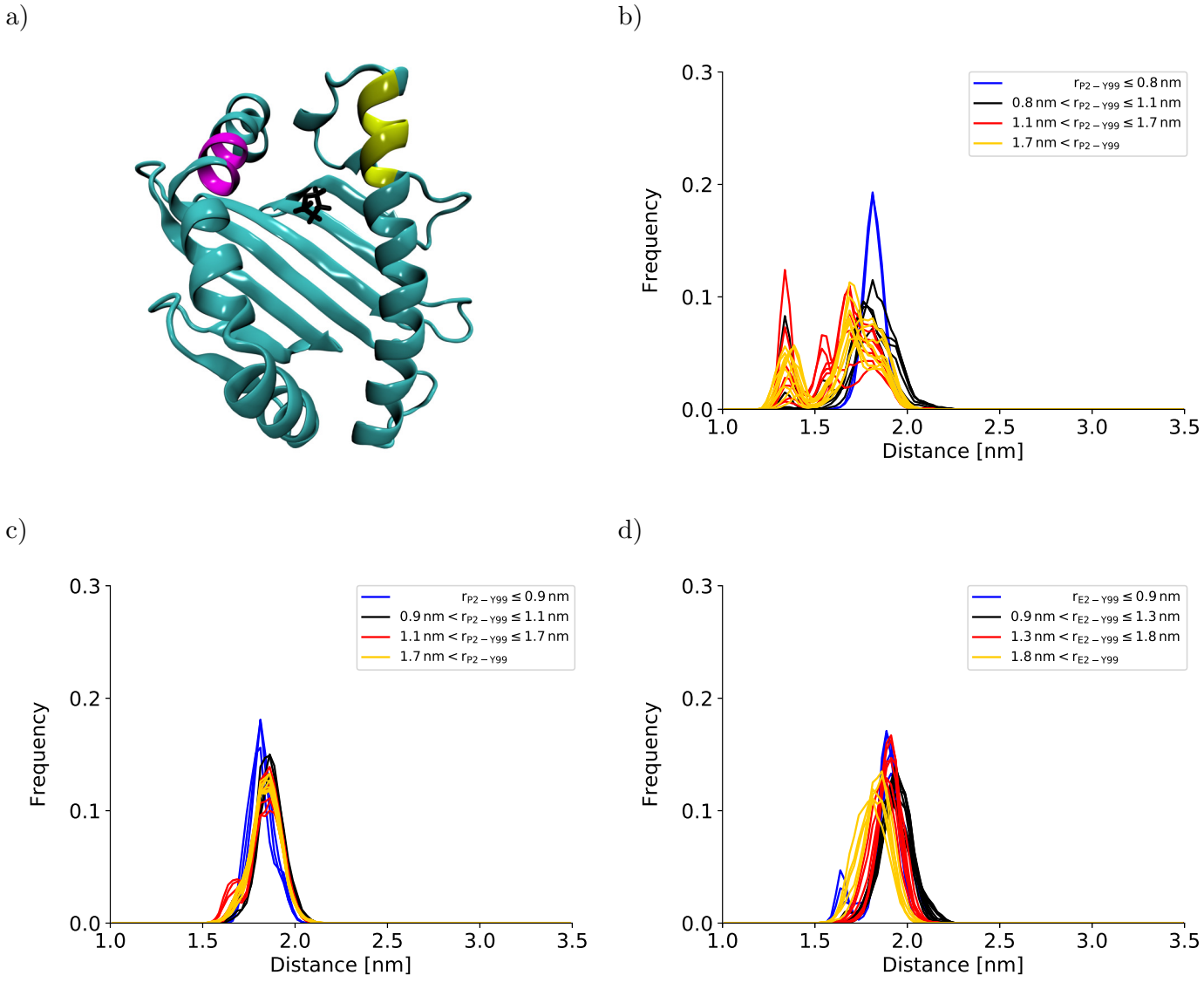

Fig. S6 Sextet distance between residues $59-64$ on the α_1-helix and residues $164-169$ on the α_2-helix. The position of the sextets in the binding groove of HLA-B*35:01 is depicted in a). The histograms of distances are shown for b) HLA-B*35:01 (starting from the final structures of the BEUS simulation performed with AMBER99SB*-ILDNP[17]), c) HLA-B*35:01 (starting from the crystal structure), and d) HLA-B*44:02 (starting from the crystal structure). Histograms shown in blue represent umbrella windows of the fully bound state, histograms in black belong to the barrier region of the PMF, and histograms in red and yellow belong to the adjacent and distant half of the partially dissociated state, respectively.

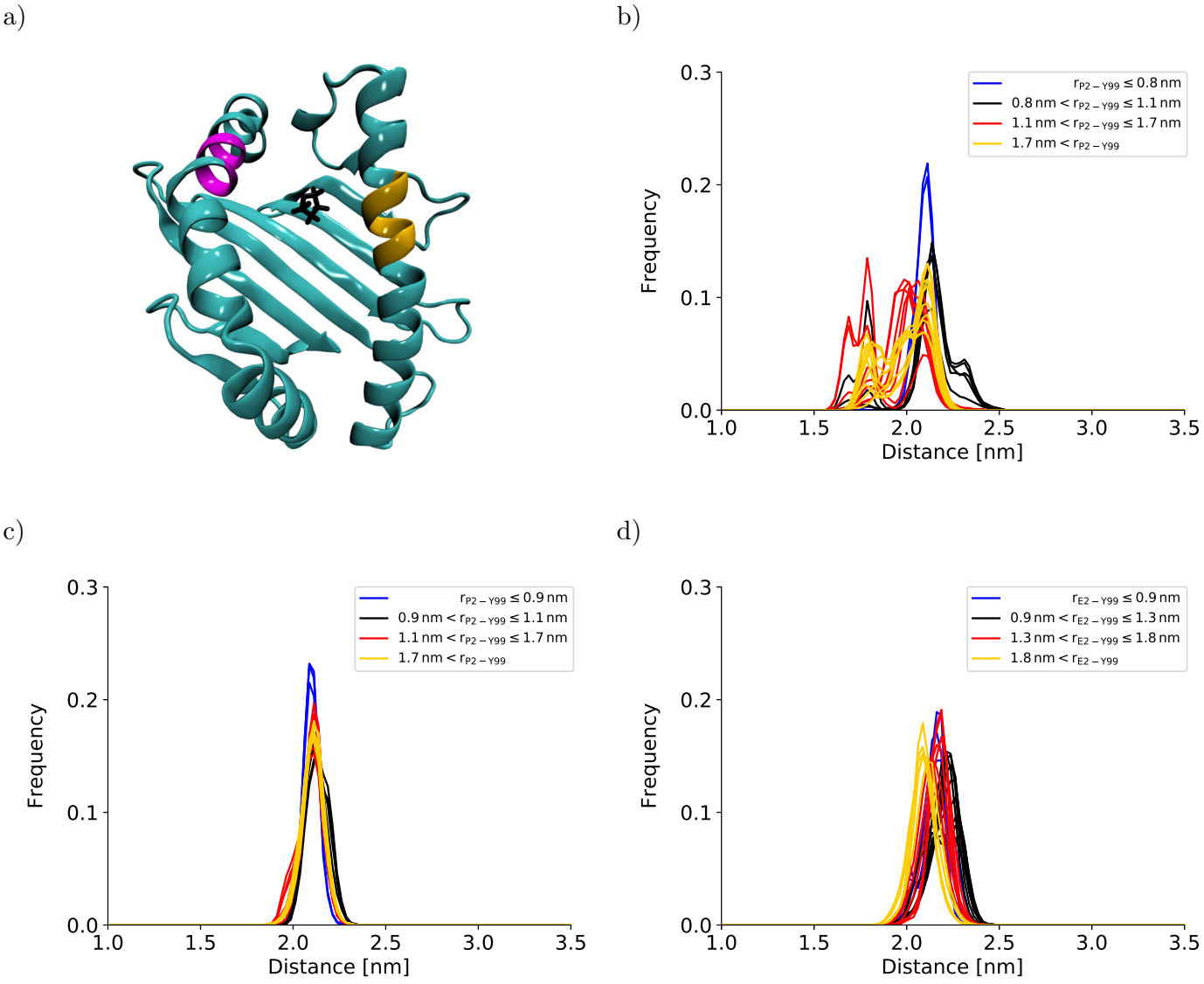

Fig. S7 Sextet distance between residues $65-70$ on the α_1-helix and residues $164-169$ on the α_2-helix. The position of the sextets in the binding groove of HLA-B*35:01 is depicted in a). The histograms of distances are shown for b) HLA-B*35:01 (starting from the final structures of the BEUS simulation performed with AMBER99SB*-ILDNP[17]), c) HLA-B*35:01 (starting from the crystal structure), and d) HLA-B*44:02 (starting from the crystal structure). Histograms shown in blue represent umbrella windows of the fully bound state, histograms in black belong to the barrier region of the PMF, and histograms in red and yellow belong to the adjacent and distant half of the partially dissociated state, respectively.

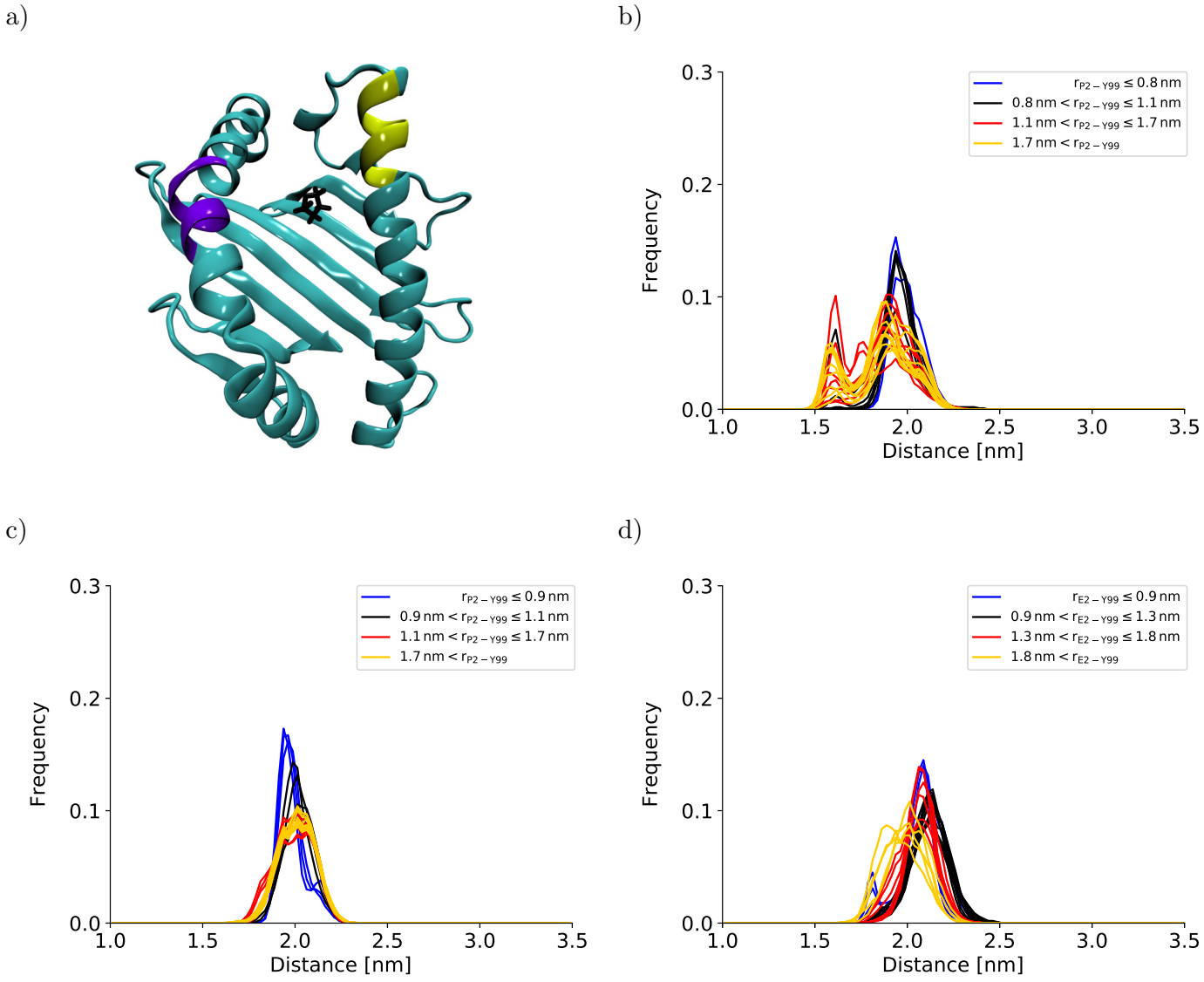

Fig. S8 Sextet distance between residues $59-64$ on the α_1-helix and residues $158-163$ on the α_2-helix. The position of the sextets in the binding groove of HLA-B*35:01 is depicted in a). The histograms of distances are shown for b) HLA-B*35:01 (starting from the final structures of the BEUS simulation performed with AMBER99SB*-ILDNP[17]), c) HLA-B*35:01 (starting from the crystal structure), and d) HLA-B*44:02 (starting from the crystal structure). Histograms shown in blue represent umbrella windows of the fully bound state, histograms in black belong to the barrier region of the PMF, and histograms in red and yellow belong to the adjacent and distant half of the partially dissociated state, respectively.

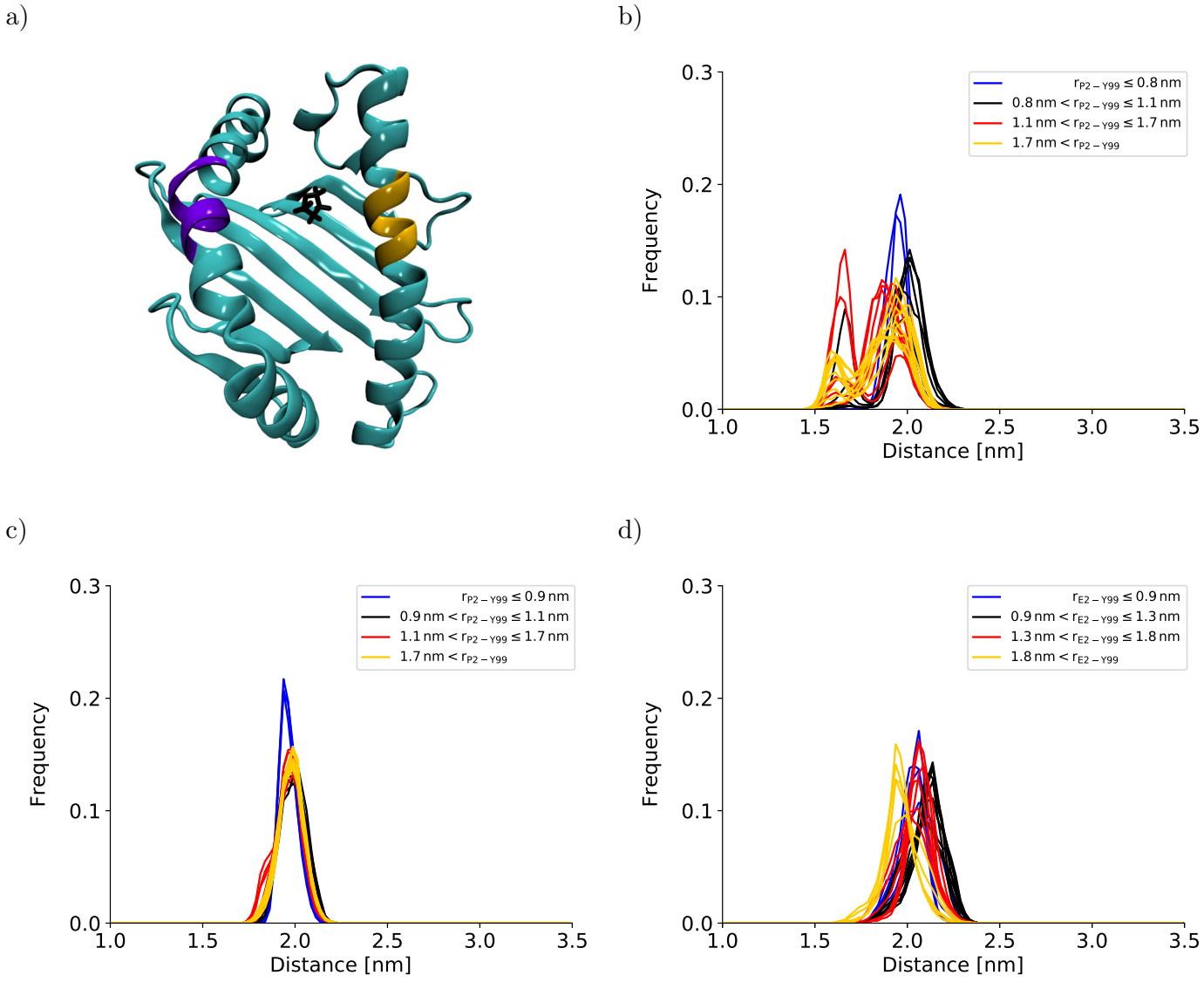

Fig. S9 Sextet distance between residues $65-70$ on the α_1-helix and residues $158-163$ on the α_2-helix. The position of the sextets in the binding groove of HLA-B*35:01 is depicted in a). The histograms of distances are shown for b) HLA-B*35:01 (starting from the final structures of the BEUS simulation performed with AMBER99SB*-ILDNP[17]), c) HLA-B*35:01 (starting from the crystal structure), and d) HLA-B*44:02 (starting from the crystal structure). Histograms shown in blue represent umbrella windows of the fully bound state, histograms in black belong to the barrier region of the PMF, and histograms in red and yellow belong to the adjacent and distant half of the partially dissociated state, respectively.

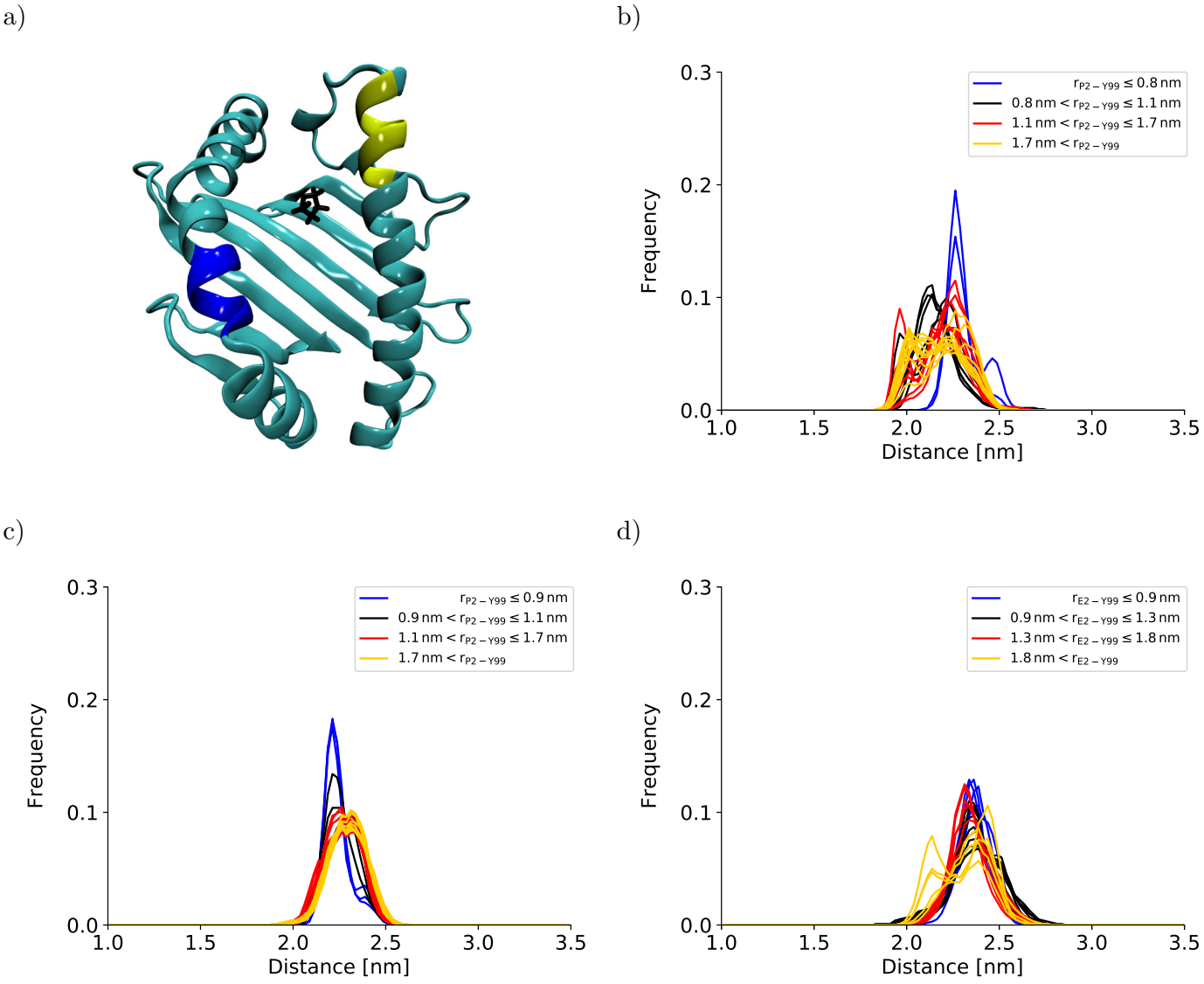

Fig. S10 Sextet distance between residues $59-64$ on the α_1-helix and residues $152-157$ on the α_2-helix. The position of the sextets in the binding groove of HLA-B*35:01 is depicted in a). The histograms of distances are shown for b) HLA-B*35:01 (starting from the final structures of the BEUS simulation performed with AMBER99SB*-ILDNP[17]), c) HLA-B*35:01 (starting from the crystal structure), and d) HLA-B*44:02 (starting from the crystal structure). Histograms shown in blue represent umbrella windows of the fully bound state, histograms in black belong to the barrier region of the PMF, and histograms in red and yellow belong to the adjacent and distant half of the partially dissociated state, respectively.

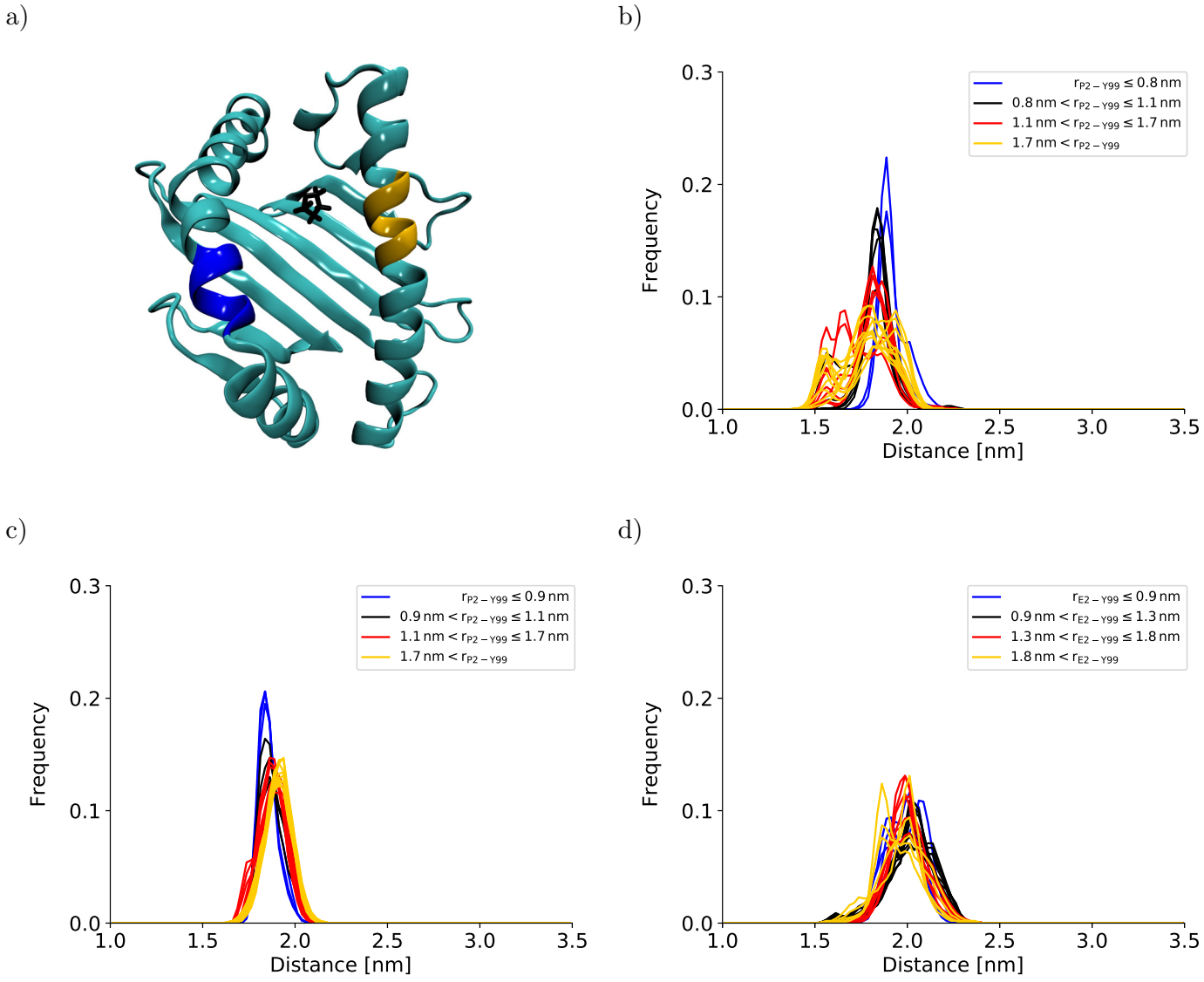

Fig. S11 Sextet distance between residues $65-70$ on the α_1-helix and residues $152-157$ on the α_2-helix. The position of the sextets in the binding groove of HLA-B*35:01 is depicted in a). The histograms of distances are shown for b) HLA-B*35:01 (starting from the final structures of the BEUS simulation performed with AMBER99SB*-ILDNP[17]), c) HLA-B*35:01 (starting from the crystal structure), and d) HLA-B*44:02 (starting from the crystal structure). Histograms shown in blue represent umbrella windows of the fully bound state, histograms in black belong to the barrier region of the PMF, and histograms in red and yellow belong to the adjacent and distant half of the partially dissociated state, respectively.

3 Schlitter Entropies

To complement the Schlitter entropies for the binding groove shown in Figure 4, the Schlitter entropies for the antigenic peptide only and for the binding groove together with the antigenic peptide are provided here.

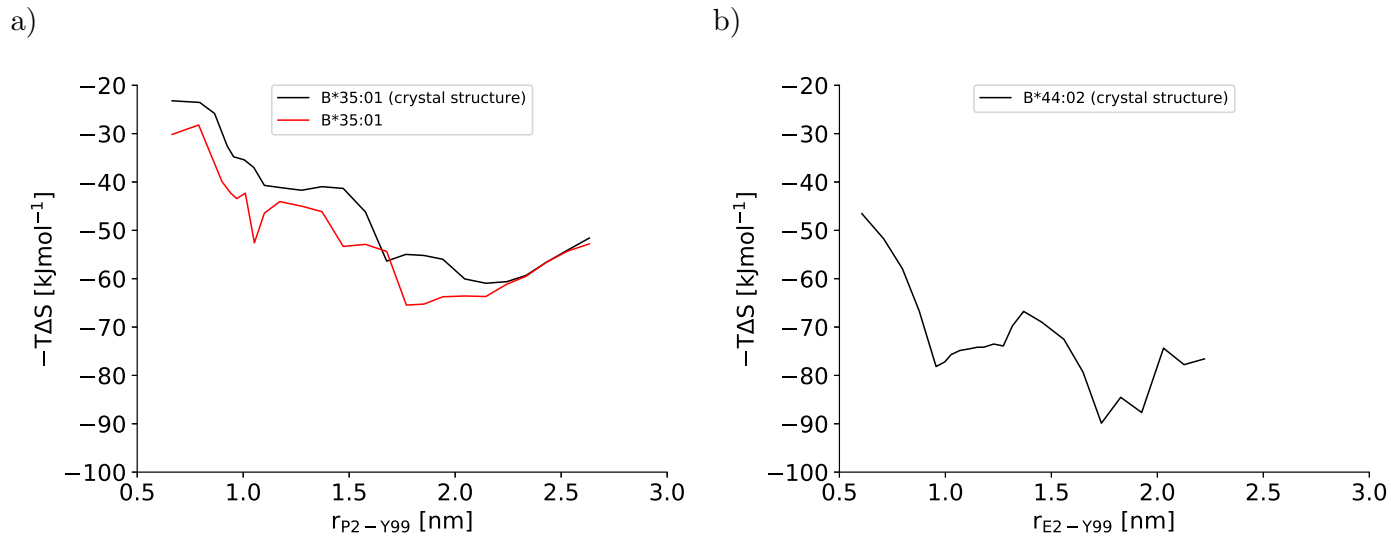

Fig. S12 Configurational entropy of the antigenic peptide obtained with the Quasiharmonic Approximation (QHA) as formulated by Schlitter[19] for a) HLA-B*35:01 and b) HLA-B*44:02.

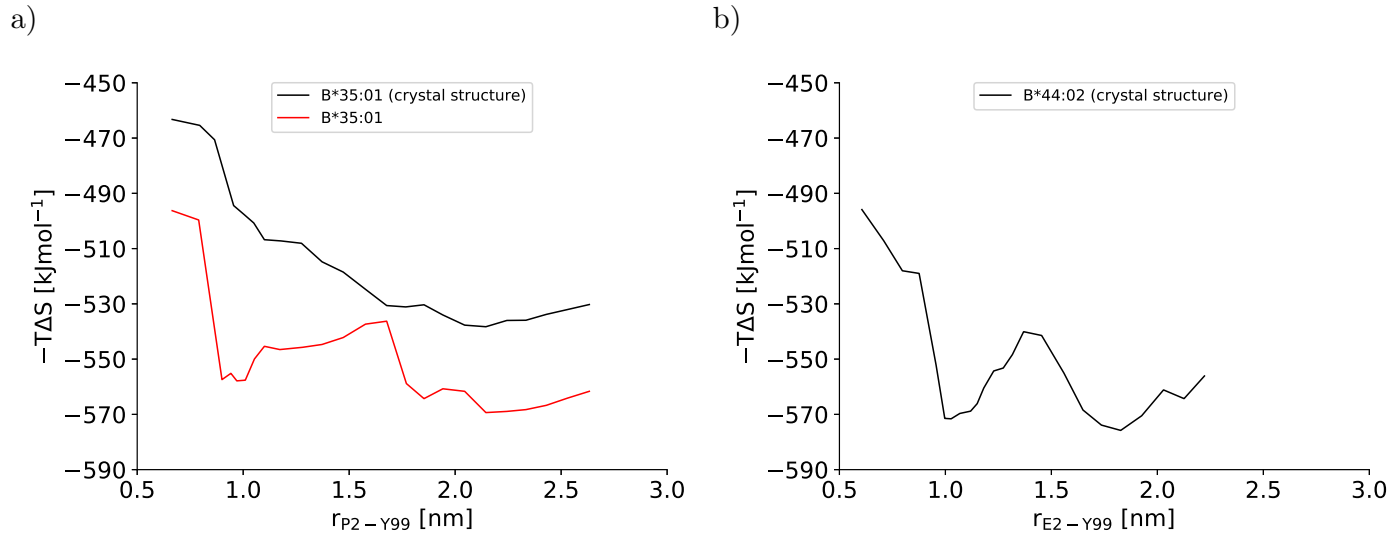

Fig. S13 Configurational entropy of the binding groove and the antigenic peptide together obtained with the Quasiharmonic Approximation (QHA) as formulated by Schlitter[19] for a) HLA-B*35:01 and b) HLA-B*44:02. Schlitter entropies are not additive such that the entropies shown here are not the sum of the Schlitter entropy for the peptide and the Schlitter entropy for the binding groove.

References

1 M. J. Abraham, T. Murtola, R. Schulz, S. Páll, J. C. Smith, B. Hess and E. Lindahl, *SoftwareX*, 2015, **1–2**, 19–25.

2 S. Páll, M. J. Abraham, C. Kutzner, B. Hess and E. Lindahl, *Solving Software Challenges for Exascale*, 2015, **8759**, 3–27.

3 S. Pronk, S. Páll, R. Schulz, P. Larsson, P. Bjelkmar, R. Apostolov, M. R. Shirts, J. C. Smith, P. M. Kasson, D. van der Spoel, B. Hess and E. Lindahl, *Bioinformatics*, 2013, **29**, 845–854.

4 B. Hess, C. Kutzner, D. van der Spoel and E. Lindahl, *J. Chem. Theory Comput.*, 2008, **4**, 435–447.

5 D. van der Spoel, E. Lindahl, B. Hess, G. Groenhof, A. E. Mark and H. J. C. Berendsen, *J. Comput. Chem.*, 2005, **26**, 1701–1718.

6 E. Lindahl, B. Hess and D. van der Spoel, *J. Mol. Model.*, 2001, **7**, 306–317.

7 H. J. C. Berendsen, D. van der Spoel and R. van Drunen, *Comp. Phys. Comm.*, 1995, **91**, 43–56.

8 G. A. Tribello, M. Bonomi, D. Branduardi, C. Camilloni and G. Bussi, *Comput. Phys. Commun.*, 2014, **185**, 604–613.

9 P. Robustelli, S. Piana and D. E. Shaw, *Proc. Natl. Acad. Sci. U. S. A.*, 2018, **115**, E4758–E4766.

10 S. Piana, A. G. Donchev, P. Robustelli and D. E. Shaw, *J. Phys. Chem. B*, 2015, **119**, 5113–5123.

11 U. Essmann, L. Perera, M. L. Berkowitz, T. Darden, H. Lee and L. G. Pedersen, *J. Chem. Phys.*, 1995, **103**, 8577–8593.

12 B. Hess, H. Bekker, H. J. C. Berendsen and J. G. E. M. Fraaije, *J. Comput. Chem.*, 1997, **18**, 1463–1472.

13 B. Hess, *J. Chem. Theory Comput.*, 2008, **4**, 116–122.

14 S. Miyamoto and P. A. Kollman, *J. Comput. Chem.*, 1992, **13**, 952–962.

15 G. Bussi, D. Donadio and M. Parrinello, *J. Chem. Phys.*, 2007, **126**, 014101.

16 H. J. C. Berendsen, J. P. M. Postma, W. F. van Gunsteren, A. DiNola and J. R. Haak, *J. Chem. Phys.*, 1984, **81**, 3684–3690.

17 S. Wingbermühle and L. V. Schäfer, *J. Chem. Theory Comput.*, 2020, **16**, 4615–4630.

18 J. S. Hub, B. L. de Groot and D. van der Spoel, *J. Chem. Theory Comput.*, 2010, **6**, 3713–3720.

19 J. Schlitter, *Chem. Phys. Lett.*, 1993, **215**, 617–621.